40G-OCDMA-PON System With an Asymmetric Structure Using a Single Multi-Port and Sampled SSFBG Encoder/Decoders

Ryosuke Matsumoto, Takahiro Kodama, *Member, IEEE*, Satoshi Shimizu, Ryujiro Nomura, Koji Omichi, Naoya Wada, *Member, IEEE*, and Ken-Ichi Kitayama, *Fellow, IEEE*

***Abstract*—In the hybrid optical code division multiple access (OCDMA) architectures using different types of optical encoder/decoder (E/Ds) between an optical line terminal and optical network units, a hybrid 40G-OCDMA-PON with a single multi-port and super-structured fiber Bragg grating (SSFBG) E/Ds is studied as a candidate system beyond next-generation PON stage 2 (NG-PON2). In this paper, we have developed uniformed and sampled SSFBG E/Ds with different refractive index profiles and have compared their code performances in a hybrid 40G-OCDMA-PON system. The experimental results show that the sampled profile improves the code dependent performances presented in many OCDMA systems. We have also demonstrated a full-duplex 4-user $\times$ 40 Gb/s hybrid OCDMA-PON system by applying the sampled SSFBG E/Ds. An asynchronous full-duplex 50 km transmission with a total capacity of 160 Gb/s (4-user $\times$ 40 Gb/s) has been achieved for the first time. Furthermore, we focus on major requirements in NG-PON2 and discuss several issues to introduce the hybrid 40G-OCDMA-PON for optical access networks.**

***Index Terms*—Arrayed waveguide grating (AWG), optical code division multiple access (OCDMA), passive optical network (PON), super-structured fiber Bragg grating (SSFBG).**

I. Introduction

PASSIVE optical network (PON) architecture is one of the promising solutions for fiber to the home (FTTH) systems due to the cost-effective facilities. Commercial development of Gigabit PON (G-PON) and Gigabit Ethernet PON (GE-PON) are underway all over the world. To increase system capacity, Institute of Electrical and Electronics Engineers (IEEE) has completed the standardization of 10 Gigabit Ethernet PON (10GE-PON) in 2009 [1]. On the other hand, 10-Gigabit capable passive optical network (XG-PON) has been standardized by International Telecommunication Union Telecommunication Standardization sector (ITU-T) in 2010 [2]. These are categorized in the next-generation PON stage 1 (NG-PON1) after the G-PON systems, which are based on time division multiplexing/time division multiple access introduced in G-PON and GE-PON. Recently, NG-PON2 has been actively studied in full service access network [3]. Aiming at the smooth migration into current PON and NG-PON1, NG-PON2 is likely to pick up time and wavelength division multiplexing (TWDM) as a prime candidate [4]. NG-PON2 must also support at least 40 Gb/s capacity in downstream and at least 10 Gb/s capacity in upstream. As the available spectral range for TWDM technique is not sufficient to support the ever-increasing traffic in forthcoming years, a demand for the revolutionary PON architecture may be called NG-PON3 [5].

Optical code division multiple access (OCDMA) is one candidate for NG-PON3. It is noteworthy that the spectral efficiency of OCDMA can be the same as dense WDM by using the optimum filtering schemes to suppress the crosstalk effect [6]: recently, OOK-OCDMA-based 10G-PON with 0.8-b/s/Hz was reported [7]. OCDMA-PON can also provide high data confidentiality, full asynchronous transmission, and symmetric bandwidth for up- and downlink [8], [9]. In an OCDMA system, the code generation and recognition function are performed at the optical domain. Fig. 1 shows the architecture of a hybrid encoder/decoder (E/D) system using the different types of optical E/Ds between an optical line terminal (OLT) and optical network units (ONUs). The multi-port E/D has the capability of simultaneous generation and recognition of multiple time-spreading optical codes in a single device [10], which is newly developed for 40G-OCDMA system in 2011 [11]. The use of multi-port E/D can aggregate the OLT, whereas the optical E/D processing single optical code at ONU is low-cost device with small-footprint. Therefore, the hybrid approach in an OCDMA can improve the cost-effectiveness and the system flexibility for the demand of ONUs [12], [13]. A super-structured fiber Bragg grating (SSFBG) is one of the candidate for the E/D at ONU [14], which has features such as polarization independent performance, low and code length independent insertion losses, in addition to good connectivity with the optical fiber.

In this paper, we propose and demonstrate for the first time a full-duplex transmission of hybrid 40G-OCDMA-PON using a single multi-port E/D at the OLT and SSFBG E/Ds at the

Manuscript received October 31, 2013; revised December 22, 2013; accepted January 3, 2014. Date of publication January 8, 2014; date of current version January 31, 2014. This work has been funded by NICT R&D program, Basic Technologies for High-Performance Optoelectronic Hybrid Packet Router (2011–2016).

R. Matsumoto, T. Kodama, and K.-I Kitayama are with the Department of Electrical, Electronic, and Information Engineering, Osaka University, Osaka 565-0871, Japan (e-mail: mastumoto@pn.comm.eng.osaka-u.ac.jp; kodama@pn.comm.eng.osaka-u.ac.jp; kitayama@comm.eng.osaka-u.ac.jp).

S. Shimizu and N. Wada are with the Photonic Network System Laboratory, National Institute of Information and Communication Technology (NICT), Tokyo 184-8795, Japan (e-mail: sshimizu@nict.go.jp; wada@nict.go.jp).

R. Nomura and K. Omichi are with the Optics and Electronics Laboratory, Fujikura Ltd., Chiba 285-8550, Japan (e-mail: ryujiro.nomura@jp.fujikura.com; koji.omichi@jp.fujikura.com).

Color versions of one or more of the figures in this paper are available online at http://ieeexplore.ieee.org.

Digital Object Identifier 10.1109/JLT.2014.2299070

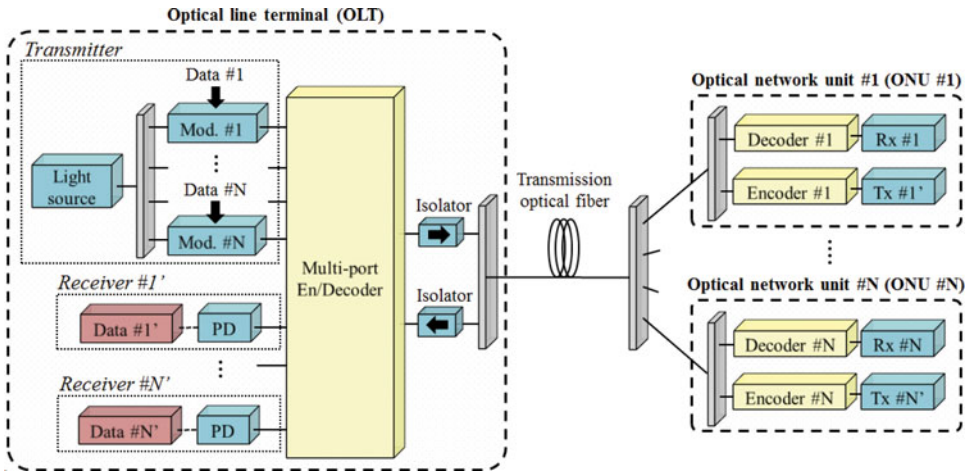

Fig. 1. Architecture of hybrid OCDMA-PON system.

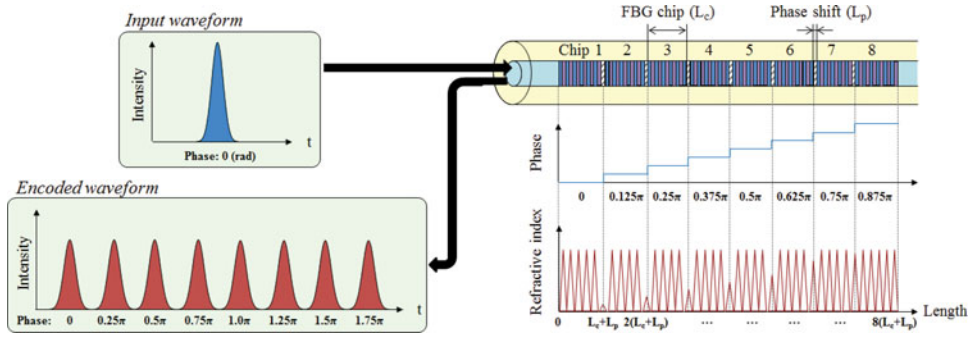

Fig. 2. Encoding principle of SSFBG.

ONUs. This paper is organized as follows. In Section II, we numerically compare the code performance between a uniformed SSFBG and non-uniformed SSFBGs with different refractive index profiles such as raised-cosine, sine^2, and sampled functions. In Section III, we develop first prototype 320 Gchip/s, 8-chip, 8-level phase-shifted uniformed and sampled SSFBG E/Ds from simulation results and investigate whether fabricated SSFBGs match the hybrid 40G-OCDMA-PON. We also demonstrate an asynchronous full-duplex 4-user $\times$ 40 Gb/s hybrid OCDMA transmission over 50 km. In Section IV, several problems in the hybrid 40G-OCDMA-PON compared with NG-PON2 are discussed from the practical points. Conclusions are presented in Section V.

II. Performance Evaluation of SSFBG E/D

A. Device Configuration

A SSFBG is defined as a special class of FBGs, in which many short grating segments along the fiber axis configure the total grating. Fig. 2 illustrates the principle of encoding by using a SSFBG. When an optical short pulse or chip pulse is injected, SSFBG encoder generates an optical code sequence by reflecting back optical chip pulses from each FBG chip. In this study, we focus on a phase-shift-keying (PSK) code categorized as a coherent code, in which the code information is embedded for the phase. Since an assignment of the multi-level code information for each chip can reduce the influence of multiple access interference (MAI) noise, the correlation property of this code is superior to other coherent code sequences [15]. To generate time-spreading PSK code in the SSFBG, it is required to adjust the number of FBG chips and the phase-shift level for desired code sequences. For example, a SSFBG is composed of eight FBG chips and 8-level phase-shift sections to match with eight chips and eight phase-level PSK code in an 8-port E/D, which encodes no phase-shifted input pulse by adding time-delays and phase-shifts in each FBG chip, as shown in Fig. 2. This SSFBG also acts as the decoder, resulting in either the autocorrelation or cross-correlation waveform according to its FBG chip arrangement.

In our previous experiment, we have demonstrated a 10G-OCDMA system using the hybrid types of single multi-port E/D and uniformed SSFBG E/Ds [12]. However, a problem remained to be solved that the bit error rate (BER) performance and the receiver sensitivities differ for code sequences. We explain this problem following the example of the hybrid OCDMA system using a multi-port encoder and SSFBG decoders, as shown in Fig. 3. In this system, an optical short pulse is transmitted from a broadband light source, encoded by the multi-port device that consists of periodic main and side lobes. The encoded signals are multiplexed at an optical coupler and recognized by each SSFBG decoder, but code performances differ due to the allocations of main lobes in the decoders. If we assume two types

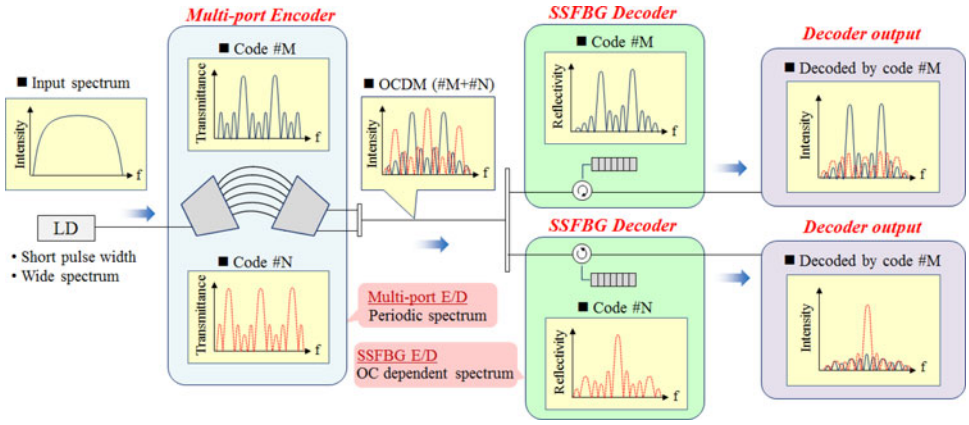

Fig. 3. Code dependence in hybrid OCDMA-PON system.

of the SSFBG decoders with two main lobes and one main lobe like codes $\#M$ and $\#N$, the decoded signal of code $\#M$ equally includes main and side lobes, whereas enhanced main lobe are observed in the signal decoded by code $\#N$. Main and side lobes mainly keeping auto- and cross-correlation signals respectively, narrow reflection spectrum such as code $\#N$ presents better code performance than other codes. Hence, this code dependent reflection causes non-uniform performances in the hybrid OCDMA systems.

To solve this problem, we introduce design approaches that control the reflection spectrum by changing the refractive index profile. Fig. 4 illustrates schematics of a reflection spectrum design. The reflection spectrum is obtained by Fourier transforming the spatial configuration of the grating [16]. If we take a SSFBG with 4-chips and 4-phase level shifts for the sake of simplicity, the reflection spectrum of uniformed SSFBG is given as the convolution of amplitude modulation (AM) and phase modulation (PM) in the frequency domain (Fig. 4(a)). The channel spacing Δf in frequency domain is expressed as

$$\Delta f = \frac{c}{2nL_{\mathrm{FBG}}} \tag{1}$$

where c is the velocity of light, n is the effective refractive index, and L_{FBG} is the interval of each FBG. Other parameters in Fig. 4(a) are the grating period Λ_0 and the Bragg frequency $f_0 = c/2n\Lambda_0$. On the other hand, reflection spectrum of the apodized SSFBG is shown in Fig. 4(b), which varies the amplitude of the refractive index along each FBG. In this case, the reflection spectrum is represented by additionally convoluting the apodized function of the refractive index change for AM and PM. When we choose an apodized profile as like Gaussian function, far main lobes from the Bragg frequency f_0 raise compared to the uniformed SSFBG. By using this apodization scheme, we have previously suppressed the dependence of code sequence [17]. However, uneven performances for code sequences still remain due to the code dependence of far main lobes enhanced by apodization technique. To completely solve this code dependent problem, we propose a new sampled SSFBG based on the concept of sampled FBG. A sampled approach is the design that exposes a pulse-like spatial refractive index profile along the FBGs [18], which can periodically allocate main lobes with same intensity to all code sequences, as shown in Fig. 4(c). In this way, the sampled SSFBG can bring out the independent decoding performance of code sequences. We designed four types of SSFBG E/Ds to match the multi-port E/D: uniformed, raised-cosine apodized, sine^2 apodized, and sampled SSFBG E/D. In this time, we select the raised-cosine and sine^2 functions from the aspect of the fabrication [19], [20]. The parameters of each SSFBG E/D are listed in Table I. Values except for the maximum index change are fixed by parameters in an 8-port E/D, whereas it is determined so as to exhibit the reflective spectrum peak of -20 dB. We also pick up four code sequences from the 8-port E/D that generates and recognizes eight orthogonal code sequences under timing synchronous condition between each code. For the eight code sequences in the 8-port E/D, these chosen four codes have the largest phase difference each other and ensure code performances in even asynchronous condition. Fig. 5 shows the normalized refractive index profiles in non-uniformed SSFBGs. Here, the sampled profile possesses the marginal width in each FBG to maintain the reproducibility. The numerical reflection spectra calculated by these parameters in Table I are shown in Fig. 6. The sampled SSFBG in Fig. 6(d) presents a flat reflectivity for all four code sequences, which is remarkably different from the other three reflection spectra that the reflectivity of the center main lobe is much larger than other main lobes as shown in Figs. 6(a)–(c). This result also shows that the design concept of Fig. 4 is valid to obtain a desired reflection spectrum in the design of SSFBG E/Ds.

B. Code Performance

To compare the performances of all code sequences generated by SSFBG E/D, we have performed numerical simulations. Fig. 7 shows the simulation model for evaluating the code performances. An optical short pulse from a mode locked laser diode (MLLD) is bandwidth-limited by an optical band pass filter (OBPF) assumed to eliminate amplified spontaneous emission (ASE) noise in the experiment. This pulse is encoded by an 8-port device that generates optical codes under the assignment of a code table. Then, the encoded signals are adjusted by attenuators (ATTs) to hold the same power and selected by an optical switch in an output of the 8-port encoder. At the

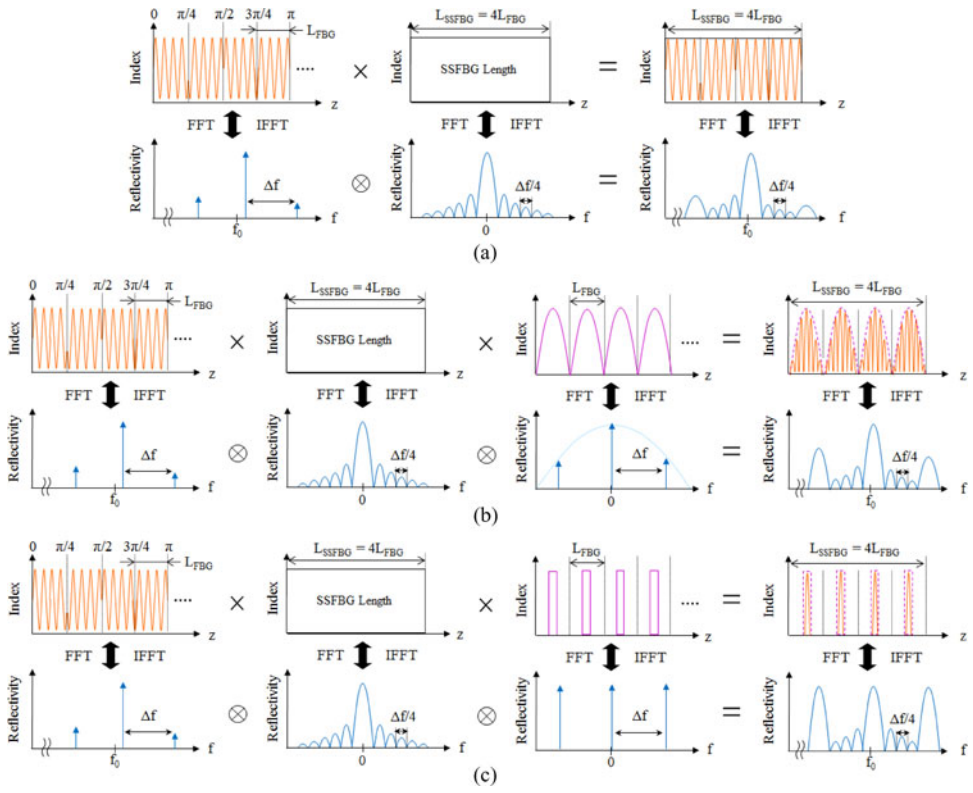

Fig. 4. Design scheme of reflection spectrum. (a) Uniformed SSFBG. (b) Apodized SSFBG. (c) Sampled SSFBG.

TABLE I
PARAMETERS USED IN NUMERICAL SIMULATIONS

Items		Uniformed SSFBG	Raised-cosine SSFBG	Sine^2 SSFBG	Sampled SSFBG
Total length of SSFBG		2.60mm			
Length of FBG chip		0.326 mm			
Number of FBG chip		8 chip			
Average effective index		1.45			
Bragg wavelength		1550 nm			
Grating period		536 mm			
code1	Phase difference	$\pi*(0.375, 0.750, 1.13, 1.50, 1.86, 2.25, 2.63, 3.00)$ rad			
	Maximum index change	2.40×10^{-5}	2.90×10^{-5}	3.40×10^{-5}	1.20×10^{-4}
code2	Phase difference	$\pi*(0.625, 1.25, 1.88, 2.50, 3.13, 3.75, 4.38, 5.00)$ rad			
	Maximum index change	2.39×10^{-5}	2.80×10^{-5}	3.30×10^{-5}	1.19×10^{-4}
code3	Phase difference	$\pi*(0.875, 1.75, 2.63, 3.50, 4.34, 5.25, 6.13, 7.00)$ rad			
	Maximum index change	1.95×10^{-5}	2.40×10^{-5}	3.00×10^{-5}	1.19×10^{-4}
code4	Phase difference	$\pi*(0.125, 0.250, 0.375, 0.500, 0.625, 0.750, 0.875, 1.00)$ rad			
	Maximum index change	2.00×10^{-5}	2.40×10^{-5}	3.10×10^{-5}	1.20×10^{-4}

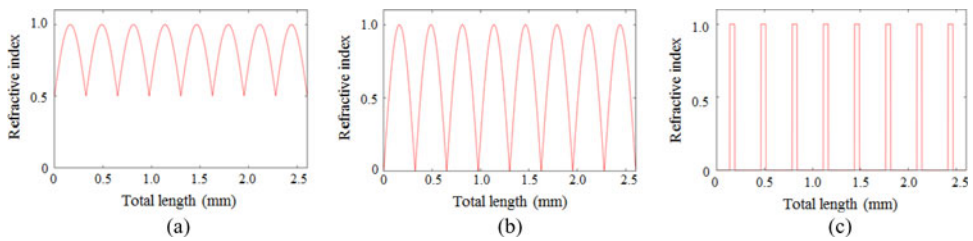

Fig. 5. Normalized refractive index profiles in non-uniformed SSFBGs. (a) Raised-cosine SSFBG. (b) Sine^2 SSFBG. (c) Sampled SSFBG.

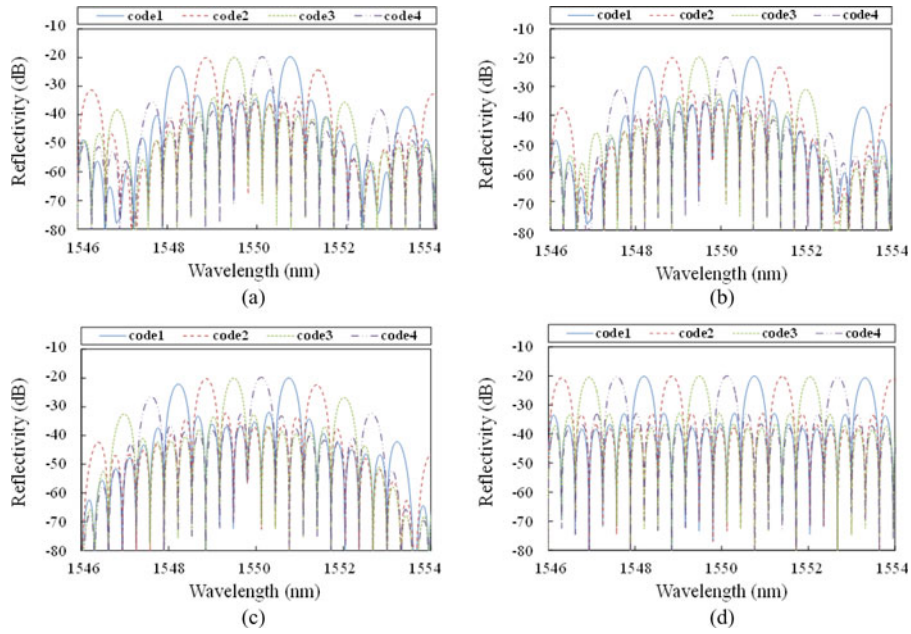

Fig. 6. Calculated reflection spectra. (a) Uniformed SSFBG. (b) Raised-cosine SSFBG. (c) Sine^2 SSFBG. (d) Sampled SSFBG.

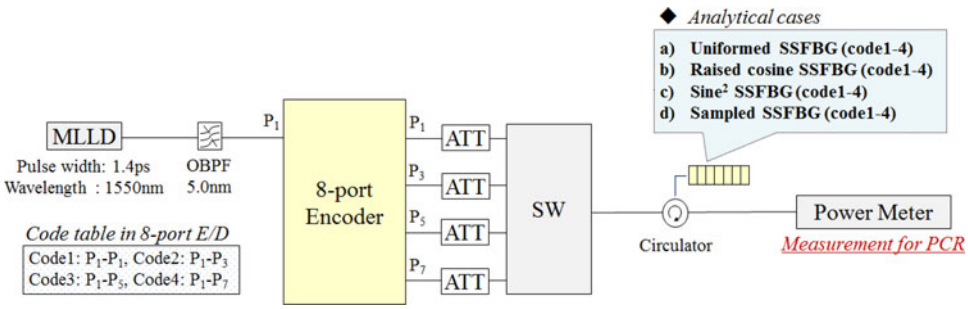

Fig. 7. Simulation model to evaluate code performances.

decoder, each SSFBG recognizes a code sequence transmitted from the 8-port encoder; autocorrelation signal can be detected if the code sequences are matched between the encoder and the decoder, otherwise cross-correlation signals are measured. We have evaluated a power contrast ratio (PCR) defined as the ratio between auto- and cross-correlation powers. Fig. 8 shows the PCRs as the function of output port number in the 8-port encoder. The PCR of uniformed SSFBGs indicate that codes 3 and 4 allocating one main lobe near the Bragg wavelength suppress the influence of interferences than codes 1 and 2 that consist of two main lobes within the bandwidth of the OBPF, as described in the schematic of Fig. 4. We can also observe a difference of 2 dB for cross-correlation averages between the worst code 2 and the best code 4, which leads to non-uniformity of BER performances. On the other hand, non-uniformed SSFBGs reduce these differences between the worst and the best ones by adjusting the intensity of main lobes in reflection spectra. A most remarkable point is that perfect even performance is confirmed in the PCRs for the sampled SSFBG, thus the use of sampled SSFBG is effective to overcome the dependence of code sequences.

III. Experimental Demonstration of Hybrid 40G-OCDMA-PON System

A. Simplex Transmission

In order to study the feasibility of the hybrid 40G-OCDMA-PON system, we have developed two types of test 320 Gchip/s, 8-chip, 8-phase-level-shifted SSFBG E/Ds, whose index profiles are uniformed and sampled functions. The choice of sampling function was decided based on the design scheme and the analytical results in Section II. These super-structured gratings are written on a conventional single mode fiber (SMF) using Ar second harmonic generation laser and phase mask. The phase-shifts are employed by controlling the relative positions between adjacent FBG chips. These fabricated SSFBGs are also inserted in 45 mm $\times$ 3 mm package without temperature control for reducing the size and the cost of ONU. Fig. 9 represents the measured reflection spectra of these SSFBGs on code 4 that is most sensitive to the phase-shift error due to the smallest phase-shift step. As can be seen in Fig. 9, the spectrum shapes of the measurement data agree well with the simulated ones. It means that the phase-shifts are precisely controlled to configure a good spectrum shape. Same characteristics are obtained for other

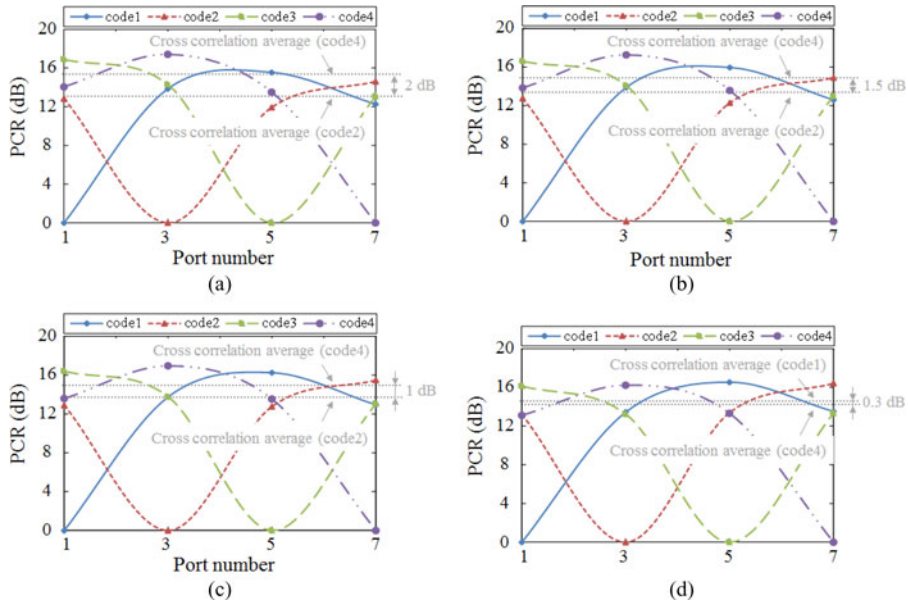

Fig. 8. Calculated PCRs. (a) Uniformed SSFBG. (b) Raised-cosine SSFBG. (c) Sine^2 SSFBG. (d) Sampled SSFBG.

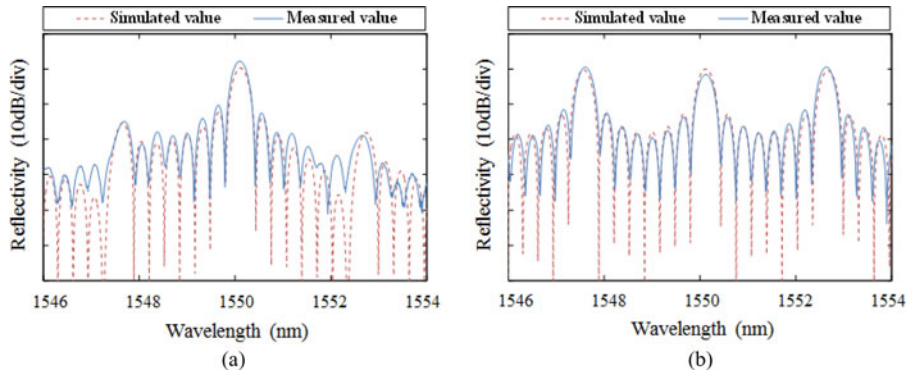

Fig. 9. Calculated and measured reflection spectra. (a) Uniformed SSFBG. (b) Sampled SSFBG.

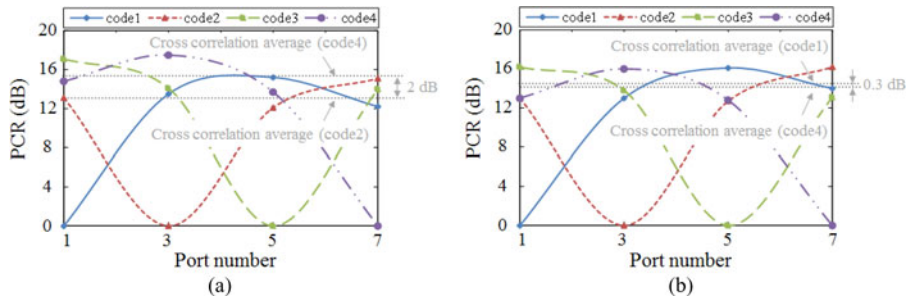

Fig. 10. Measured PCRs. (a) Uniformed SSFBG. (b) Sampled SSFBG.

optical code sequences as well. We also measured the PCRs to examine the code performance of fabricated SSFBG E/Ds, as shown in Fig. 10. Although the uniformed SSFBG shows 2 dB unevenness for cross-correlation averages of the PCRs between the worst code 2 and the best code 4, equivalent PCRs are measured for all code sequences in the sampled SSFBG. These results are in good agreement with the numerical simulations, and the PCRs of the sampled SSFBG suggest to achieve same decoding performances for each code sequence.

We have conducted an experiment of 4-user $\times$ 40 Gb/s OCDMA-PON system using an 8-port encoder and SSFBG decoders, aiming the comparison of system performances between uniformed and sampled SSFBG E/Ds. Fig. 11 shows the experimental setup and the measured waveforms in simplex downlink transmission. The transmitter (Tx) part consists of an electrical part to provide the data pattern and an optical part to generate the optical pulse sequence. At the electrical part, a pattern of $2^{31} - 1$ pseudo random bit sequence at 10 Gb/s from a pulse

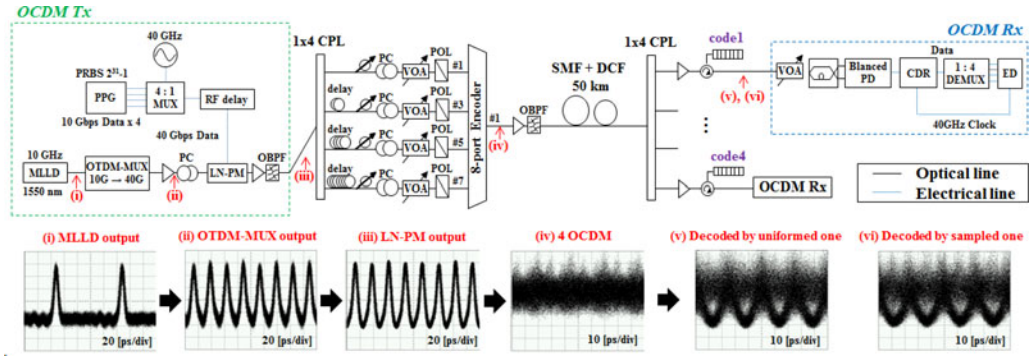

Fig. 11. Experimental setup and results to compare system performances between uniformed and sampled SSFBGs.

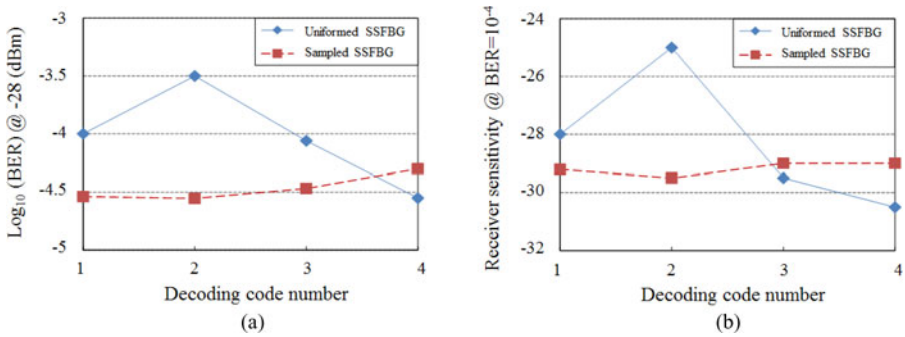

Fig. 12. Measured system performances. (a) BERs at received optical power of -28 dBm. (b) Receiver sensitivities of BER $= 10^{-4}$.

pattern generator is multiplexed to 40 Gb/s through a 10G-to-40G electrical multiplexer (4:1 MUX). At the optical part, the MLLD generates the 1.4 ps optical pulse at the repetition rate of 10 GHz and the center wavelength of 1550 nm (Fig. 11(i)). This optical pulse train is multiplexed to the 40 GHz by a 10G-to-40G optical time-division-multiplexer (OTDM-MUX), as indicated in Fig. 11(ii). The 40G pulse train is modulated by the electrical signal generated in the electrical part to make a differential phase shift keying (DPSK) signal by using a $LiNbO_3$ phase modulator (LN-PM). The phase-modulated signal shown in Fig. 11(iii) is split into four branches, and they are launched into the odd input ports of an 8-port encoder. Since this experiment assumes full asynchronous OCDMA transmission in worst-case scenario, we multiplex each encoded signal that has equal power, same polarization, and largest interfering bit phase and timing-delay with autocorrelation signal. We also place a temperature controller in the 8-port E/D and control the thermal change of the SSFBG E/Ds. This temperature controller compensates the thermal difference between temperature of the 8-port E/D and average temperature of all SSFBG decoders. By using this controller, we can precisely manage the code performances when the thermal difference between each SSFBG decoder is within 8.0 K. If the temperature range between the ONUs is larger than 8.0 K, temperature controller for the SSFBGs should be installed in each ONU. The asynchronous encoded signal multiplexed in these conditions is shown in Fig. 11(iv), transmitted in a 50 km fiber link composed of a fiber pair of a SMF and a dispersion compensated fiber (DCF). The transmitted signal is decoded by uniformed and sampled SSFBG decoders with each code sequence, and insets (v, vi) of Fig. 11 are the decoding waveforms in uniformed and sampled SSFBGs on code1. These decoded signals are detected by a DPSK receiver consisting of a Mach–Zehnder delayed interferometer and a balanced photo diode (PD) with 42 GHz of receiver bandwidth. We employ a clock-and-data recovery circuit and a 40G-to-10G electrical demultiplexer (1:4 DEMUX) after the DPSK detection and measure BERs.

We have evaluated the system performances by measuring the BER. Fig. 12(a) shows the BERs of each SSFBG decoder when the received optical power is -28 dBm determined as a minimum receiver sensitivity in 10GBASE PR-D3 [1]. Although the BER of uniformed SSFBGs ranged from 3.0×10^{-4} to 2.0×10^{-5}, the sampled SSFBGs performed even BER near about 4.0×10^{-5}. The receiver sensitivities measured as another evaluation are shown in Fig. 12(b), where the reference BER was set to 1.0×10^{-4} that drew an error-floor in the worst code. A difference of 5.5 dB was observed between the receiver sensitivities of uniformed SSFBGs, whereas the received performances of the sampled SSFBG were almost the same for all code sequences. These results match with the calculated and measured properties in the PCRs of Section II, and the sampled profile concludes to solve code dependent problem like the design scheme. We also note that the difference in the system performances would be enhanced in the higher receiver sensitivity or the lower BER.

B. *Full-Duplex Transmission*

Fig. 13 shows the experimental setup of an asynchronous full-duplex 4-user $\times$ 40G-OCDM-PON system over 50 km fiber transmission. We employed an 8-port encoder at the OLT and

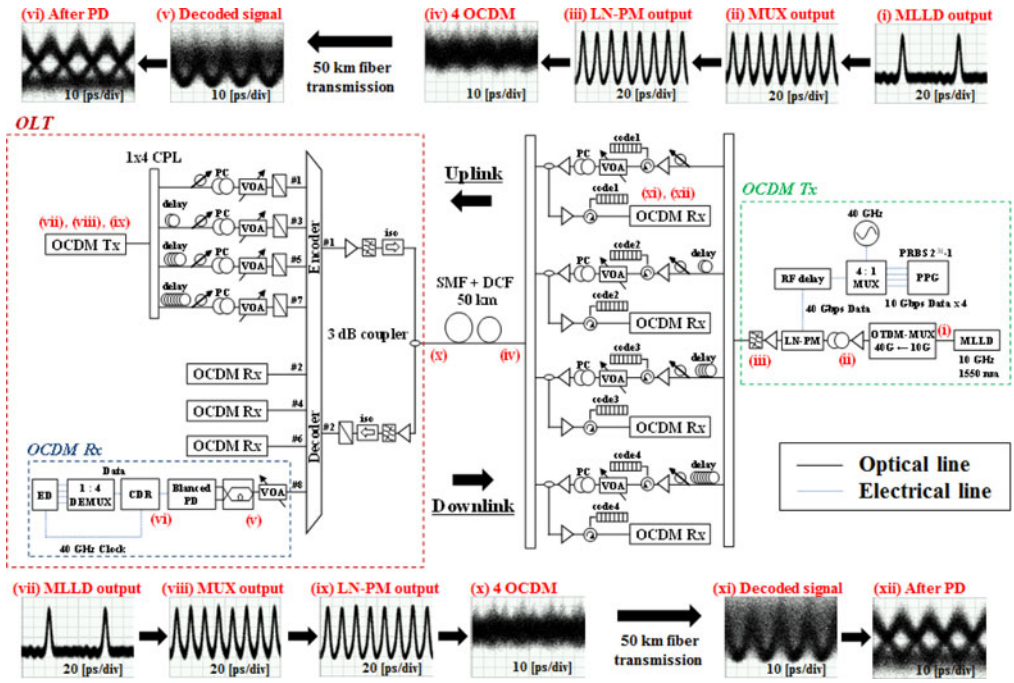

Fig. 13. Experimental setup and results of full-duplex 40G-OCDM-PON.

sampled SSFBG decoders at the ONUs, while OCDM Tx/Rx are the same configuration as Fig. 11.

In the uplink, the output waveforms of the MLLD and the OTDM-MUX are shown in the insets (i, ii) of Fig. 13. The multiplexed pulse sequence is modulated as shown in Fig. 13(iii) and this modulated data signal is sent from OCDM Tx. This pulse stream is split into four branches and launched into four different sampled SSFBG encoders to generate the optical codes. Fig. 13(iv) indicates the encoded signal in the worst case scenario. This signal is transmitted in a 50 km fiber link paired by a SMF and a DCF. Then, it is simultaneously decoded as four original signals by an 8-port decoder as shown in Fig. 13(v). The decoded signal is detected by the OCDM Rx. Fig. 13(vi) shows the detected eye diagram after going through the DPSK detector.

In the downlink, as well as the uplink, the output signals of downlink's MLLD, OTDM-MUX and LN-PM are shown in Figs. 13(vii)–(ix). This modulated signal is split into four branches with worst condition and sent to the odd input ports of the 8-port encoder that has the same codes as the 8-port decoder. These four encoded signals are combined as shown in Fig. 13(x), and transmitted through the 50 km fiber. Afterward, the signal is decoded by each sampled SSFBG decoder (Fig. 13(xi)) and received by the OCDM Rx. Fig. 13(xii) shows the detected eye diagram after passing through the DPSK detector. The performance of the system is evaluated by the eye opening and BER measurement in both up- and downlink transmissions.

Figs. 14(a) and (b) present the measured BERs of simplex single-user and four-user in back-to-back (B-to-B) transmission. Error free operation (BER $< 10^{-9}$) was confirmed for single-user case in both directions, and comparatively low BERs of less than 10^{-5} were achieved for up- and downlink in case of the four-user. Figs. 14(c) and (d) also show measured BERs of simplex single-user and four-user, and full-duplex four-user

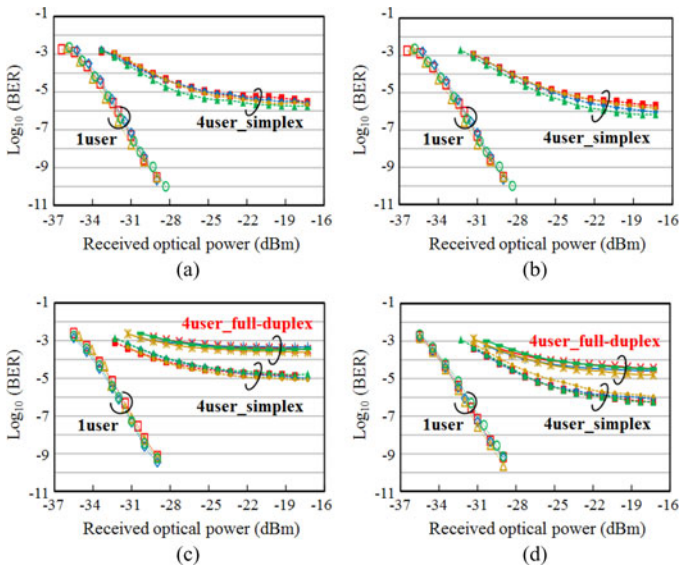

Fig. 14. Measured BERs of full-duplex 40G-OCDMA-PON. (a) Uplink in case of B-to-B. (b) Downlink in case of B-to-B. (c) Uplink over 50 km transmission. (d) Downlink over 50 km transmission.

after 50 km fiber transmission. In the uplink, single-user reaches error free operations and the BERs of less than 1.0×10^{-5} and 5.0×10^{-4} were observed in simplex and full-duplex transmission of four-user, respectively. Since simplex and full-duplex performances are the same in the SMF transmission without the DCF [21], the performance difference between simplex and full-duplex transmission in this experiment is caused by the reflection at a spliced point of the SMF and the DCF. In the downlink, as well as the uplink, error-free operations were performed for all code sequences in the single-user, and

slightly lower BER than that of the uplink was obtained for the four-user case in both simplex and full-duplex transmission. It is evident that BER performances of less than 5.0×10^{-4} were achieved even in 50 km fiber transmission, therefore this result suggests to realize an error free operation when the 7%-overhead forward error correction (FEC) is employed in the system. The degraded code-orthogonality generated by the worst-case scenario causes MAI and beat noises, which limits the performances in the OCDMA system and leads the power penalty between single-user and multiple-users.

IV. Discussion

Commercial PONs, 10G-EPON, and XG-PON employ TDM technique, which are largely cost-effective due to the simple timeslot-based protocol. NG-PON2 based on TWDM method can support many users by overlaying WDM technique with TDM system. In our hybrid 40G-OCDMA-PON, the shortcomings compared with these systems are to require the expensive light source and the additional devices such as many EDFAs at ONU, optical E/Ds, and dispersion compensator. In addition, our system can only support 4-user because of the high bit-rate per user. However, high spectral efficiency with asynchronous condition should be emphasized as the unique advantage of OCDMA-PON. In this section, we take some examples of the major requirement in NG-PON2 and discuss the solutions to realize the hybrid 40G-OCDMA-PON under these requirements.

A. Scaling ONU Number

The number of users in our OCDMA-PON system was limited to 4-user because of MAI and beat noises caused by the worst-case scenario. To accommodate more users, we must enhance the code-efficiency and combine the WDM technique with the hybrid 40G-OCDMA-PON. Recently, we have analytically used all code sequences of the 16-port E/D in an OCDMA system using the cascaded 16-port E/Ds to suppress MAI noise [7]. The accommodation of 32-user was also achieved in a 40G-WDM-OCDMA-PON with 8 wavelengths $\times$ 4 code sequences [22]. By using the cascade E/D technique, this system can accommodate 64-user (8 wavelengths $\times$ 8 codes) that satisfies the requirement of NG-PON2.

B. Dispersion Compensation

The fiber reach capability of NG-PON2 should be at least 40 km [3], and system reach of 100 km will be covered in the long-reach option [23]. To transmit the OCDMA signals in 40 or 100 km fiber link, we must compensate the influence of chromatic dispersion that strongly distorts the encoded signals with broad spectrum. To overcome this issue, two approaches are proposed and investigated in the OCDMA-PON without high-cost DCF and long chirped FBG. First one is the installation of the narrow band (NB-) OBPF to suppress chromatic dispersion. In a 10G-OCDMA-PON system using NB-OBPF, 100 km SMF transmission has been experimentally achieved under FEC limit of 10^{-3} [24]. Another approach is the dispersion compensation using the multi-channel FBG that arranges short chirped FBGs in series. This multi-channel FBG can be simply designed in comparison with long chirped FBG, which has perfectly compensated chromatic dispersion for the 10G-OCDMA signal after 80 km SMF transmission [25]. Both techniques are recommend to extend transmission distance in the 10G-OCDMA-PON system. However, the only multi-channel FBG compensator is suitable for the hybrid 40G-OCDMA-PON because it is difficult to suppress the dispersion of broad bandwidth in the filtering scheme. This FBG compensator recovers the dispersion effect with accuracy; therefore, it will be possible to realize 80 km SMF transmission in the hybrid 40G-OCDMA-PON as well as the 10G-OCDMA-PON. By improving this device, we will be able to investigate the further extension of transmission distance and expect to cover 100 km required in the long-reach system for NG-PON2. Although the additional device such as multi-channel FBG results in the cost-increase at ONUs, we can solve this problem by fabricating and placing the multi-channel FBG compensator with SSFBG E/Ds.

C. Power Budget

Network coverage and ONU cost for PON system has a dependence on the power distribution between an OLT and ONUs. To compare the power distributions of NG-PON2 and the hybrid 40G-OCDMA-PON, we calculated power consumption in each stage. The power distribution in NG-PON2 is shown in Fig. 15(a). In this calculation, we put on fiber loss of 1 dB between a splitter and the ONUs, 50 km transmission loss of 10 dB, and system margin of 3 dB. Referring these studies [4], [26], ONU Tx power and OLT Rx sensitivity are determined as 4 dBm and -35.5 dBm, respectively. We also define the power difference between received power and Rx sensitivity, as a power margin that evaluates the validity of systems. As shown in Fig. 15(a), NG-PON2 has the power budget of 37.5 dB, which keeps the power margin of 7.5 dB under 64-user accommodation without an optical amplifier. Fig. 15(b) indicates the power distribution in our 4-user $\times$ 40 Gb/s hybrid OCDMA-PON system corresponding to the experimental setup of Fig. 13. Here, Rx sensitivity of -30 dBm is referred as the minimum received optical power to achieve FEC limit. Our system obtains the large power margin of 15.3 dB, but deployment and operation of four EDFAs at an ONU are not reasonable. These EDFAs are mainly inserted to compensate low-power MLLD, OTDM-MUX loss, and SSFBG loss, which will be removed by replacing high-power MLLD and low-loss SSFBG. Fig. 15(c) shows the power distribution of ideal condition using a high-power MLLD of 15 dBm [27] and a low-loss SSFBG of 6.7 dB [28], [29]. We can confirm the sufficient power margin of 4.3 dB; at the same time, this result reveals to realize our system without EDFAs at the ONUs. Finally, we expand the discussion for a 64-user $\times$ 40 Gb/s hybrid OCDMA-PON with 8 wavelengths $\times$ 8 code sequences. To address the simple discussion, we assume the only additional splitter loss and the AWG filter loss for the consideration of Fig. 15(c). In this system, a low insertion-loss AWG filter (5 dB) [30] is placed to separate wavelengths in an OLT, and another parameters are also the same condition as Fig. 15(c). We can observe that an EDFA at a splitter shared by the ONUs

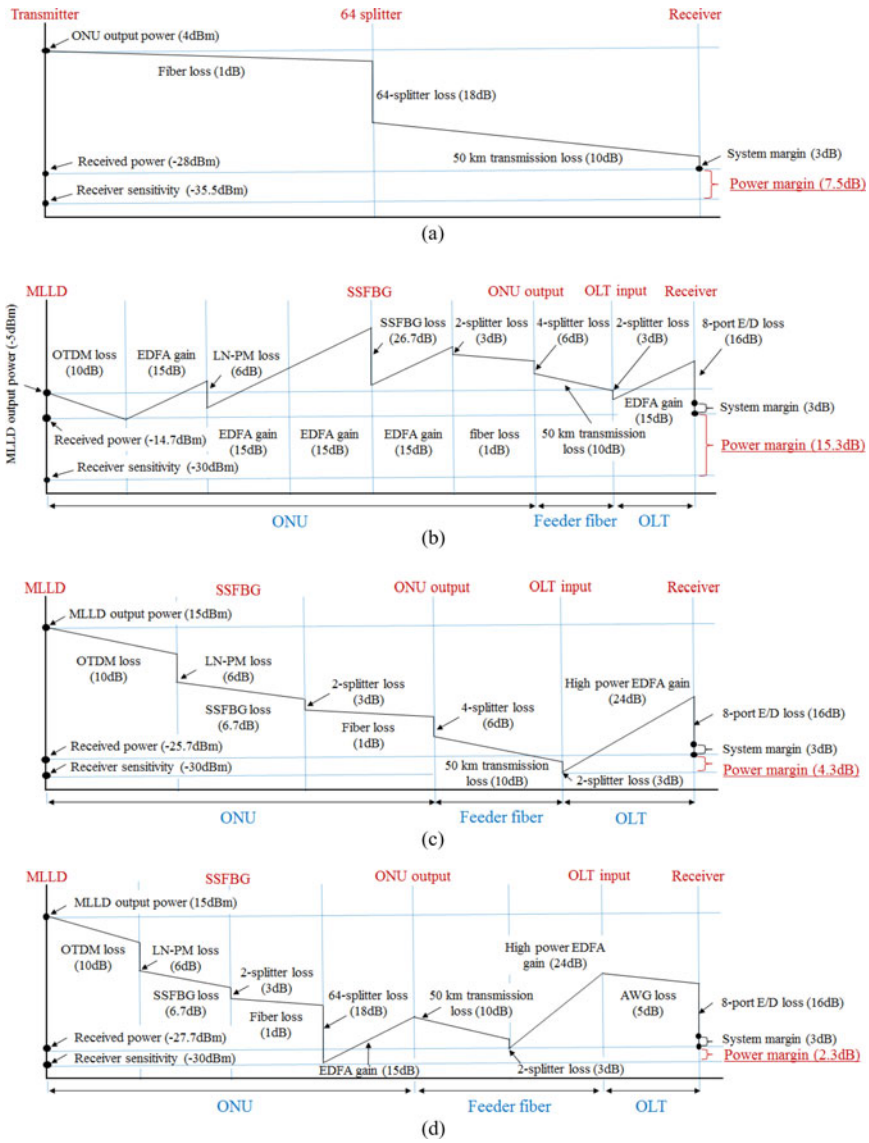

Fig. 15. Power distributions. (a) NG-PON2. (b) 4-user × 40 Gb/s hybrid OCDMA-PON in our experiment. (c) 4-user × 40 Gb/s hybrid OCDMA-PON with ideal MLLD and SSFBG E/Ds. (d) 64-user × 40 Gb/s WDM-OCDMA-PON with ideal MLLD and SSFBG E/Ds.

is required to accommodate many users in hybrid 40G-WDM-OCDMA-PON, as shown in Fig. 15(d). Hence, the complexity of the hybrid OCDMA-PON compared with NG-PON2 produces the system loss, which limits the network scale in our system. In Fig. 15(d), the primary reason for operating an EDFA at the ONU side is the compensation of low ONU output power and the 8-port E/D loss. To extend the coverage of systems based on the hybrid 40G-OCDMA-PON, it will be important to reduce the total loss in the system, by aggregating an OCDM Tx and improving the performance of optical E/D. In this section, we have treated only uplink transmission because an avalanche PD (APD) was applied in our experiment.

D. Cost Performance

Main challenge to conduct NG-PON2 is the cost-reduction at ONUs, and the use of low-cost Tx or colorless ONU is well known as the low-cost solution. In these two approaches, former one is effective to address the accommodation of many users, the extension of transmission distance, and the co-existence of legacy optical distribution network in the requirements of NG-PON2. From the same reason, our hybrid 40G-OCDMA-PON should also work on the cost-reduction of the Tx at ONUs. NG-PON2 can overcome this problem by developing high-productive lasers such as tunable distributed feedback (DFB) laser, tunable distributed Bragg reflector (DBR), and vertical-cavity surface-emitting laser (VCSEL). On the other hand, the Tx of OCDMA-PON requires an expensive optical short pulse laser corresponding to the MLLD. This system also involves the optical E/Ds as an additional device. As an evident thing from these comparisons, the cost-effectiveness of the hybrid 40G-OCDMA-PON is inferior to that of NG-PON2. By developing the high-productive SSFBG E/Ds, we have dealt with the cost-reduction of the ONUs in this study; thus, remaining key issue to introduce OCDMA-PON will be reducing the cost of laser source.

V. Conclusion

We have developed two types of SSFBG E/Ds in which index profiles are uniformed and sampled functions. The performance improvement using the sampled profile was experimentally verified. We also have demonstrated a full-duplex 4-user $\times$ 40 Gb/s hybrid OCDMA-PON system arranging a single 8-port E/D and sampled SSFBG E/Ds. An asynchronous full-duplex transmission in 50 km fiber link with the BERs under FEC limit of 10^{-3} for all code sequences has been achieved for the first time, whose total capacity has reached 160 Gb/s (4-user $\times$ 40 Gb/s). Finally, the system and device requirements of the hybrid 40G-OCDMA-PON have been summarized from the practical points.

Acknowledgment

The authors would like to thank Y. Terada, N. Asaumi, and K. Goto of Fujikura for the device fabrication. They would also like to thank Y. Tomiyama and H.Sumimoto of NICT for their support in this experiment.

References

[1] *Physical Layer Specifications and Management Parameters for 10 Gb/s Passive Optical Networks*, IEEE Std. 802.3av-2009.

[2] *10-Gigabit-Capable Passive Optical Network (XG-PON) systems*, ITU-T Recommendation G987.

[3] P. Chanclou, A. Cui, F. Geihardt, H. Nakamura, and D. Nesset, "Network operator requirements for the next generation of optical access networks," *IEEE Netw.*, vol. 26, no. 2, pp. 8–14, Mar. 2012.

[4] Y. Luo, X. Zhou, F. Effenbeger, X. Yan, G. Peng, Y. Qian, and Y. Ma, "Time- and wavelength-division multiplexed passive optical network (TWDM-PON) for next-generation PON stage 2 (NG-PON2)," *J. Lightw. Technol.*, vol. 31, no. 4, pp. 587–593, Feb. 2013.

[5] H. Nakamura, "NG-PON2 technology," in *Proc. Opti. Fiber Comumun. Conf. Nat. Fiber Opt. Eng. Conf.*, Mar. 2013, pp. 1–51, Paper Nth4F.5.

[6] T. Kodama, N. Wada, G. Cincotti, X. Wang, and K. Kitayama, "Noise suppression using optimum filtering of OCs generated by a multiport encoder/decoder," *Opt. Exp.*, vol. 20, no. 9, pp. 10320–10329, Apr. 2012.

[7] T. Kodama, N. Wada, G. Cincotti, and K. Kitayama, "Asynchronous OCDM-based 10 G-PON using cascaded multiport E/Ds to suppress MAI noise," *J. Lightw. Technol.*, vol. 31, no. 20, pp. 3258–3266, Oct. 2013.

[8] P. Prucnal, *Optical Code Divison Muliple Access*, 1st ed. Boca Raton, FL, USA: CRC Press, 2005.

[9] K. Kitayama, X. Wang, and N. Wada, "OCDMA over WDM PON-solution path to gigabit-symmetric FTTH," *J. Lightw. Technol.*, vol. 24, no. 4, pp. 1654–1662, Apr. 2006.

[10] G. Cincotti, N. Wada, and K. Kitayama, "Characterization of a full encoder/decoder in the AWG configuration for code-based photonic routers—Part I: Modeling and design," *J. Lightw. Technol.*, vol. 24, no. 1, pp. 103–112, Jan. 2006.

[11] N. Kataoka, G. Cincotti, N. Wada, and K. Kitayama, "Demonstration of asynchronous, 40 Gbps $\times$ 4-user DPSK-OCDMA transmission using a multi-port encoder/decoder," *Opt. Exp.*, vol. 19, no. 26, pp. 965–970, Dec. 2011.

[12] N. Kataoka, N. Wada, X. Wang, G. Cincotti, A. Sakamoto, Y. Terada, T. Miyazaki, and K. Kitayama, "Field trial of duplex, 10 Gbps $\times$ 8-user DPSK-OCDMA system using a single 16 $\times$ 16 multi-port encoder/decoder and 16-level phase-shifted SSFBG encoder/decoders," *J. Lightw. Technol.*, vol. 27, no. 3, pp. 299–305, Feb. 2009.

[13] S. Yoshima, N. Nakagawa, N. Kataoka, N. Suzuki, M. Noda, M. Nogami, J. Nakagawa, and K. Kitayama, "10 Gb/s-based PON over OCDMA uplink burst transmission using SSFBG encoder/multi-port decoder and burst-mode receiver," *J. Lightw. Technol.*, vol. 25, no. 4, pp. 365–371, Feb. 2010.

[14] P. C. Teh, M. Ibsen, P. Petropoulos, and D. J. Richardson, "Demonstration of a four-channel WDM/OCDMA systme using 255-chip 320-Gchip/s quaternary phase coding gratings," *IEEE. Photon. Technol. Lett.*, vol. 14, no. 2, pp. 227–229, Feb. 2002.

[15] G. Manzacca, A. Maria, X. Wang, N. Wada, G. Cincotti, and K. Kitayama, "Performance analysis of a multiport encoder/decoder in OCDMA senario," *J. Sel. Quantum Electron.*, vol. 13, no. 5, pp. 1415–1421, Sep. 2007.

[16] K. O. Hill and G. Meltz, "Fiber Bragg grating technology fundamentals and overview," *J. Lightw. Technol.*, vol. 15, no. 8, pp. 1263–1274, Aug. 1997.

[17] N. Kataoka, X. Wang, N. Wada, G. Cincotti, Y. Terada, and K. Kitayama, "8 $\times$ 8 full-duplex demonstration of asynchronous, 10 Gbps, DPSK-OCDMA system using apodized SSFBG and multi-port en/decoder," in *Proc. Eur. Conf. Opt. Commun.*, Sep. 2009, paper no. 655, pp. 1–2.

[18] Y. Nasu and S. Yamashita, "Densification of sampled fiber Bragg gratings using multiple-phase-shift (MPS) technique," *J. Lightw. Technol.*, vol. 23, no. 4, pp. 1808–1817, Apr. 2005.

[19] M . Lima, A. Teixeria, and J. Rocha, "Optimization of apodized fiber grating filters for WDM systems," in *Proc. 12th Annu. Meeting IEEE Lasers Electro-Opt. Soc.*, Nov. 1999, pp. 876–877, Paper Thz2.

[20] S. Ugale and V. Mishra, "Fiber Bragg grating modeling, characterization and optimization with different index profiles," *J. Eng. Sci. Technol.*, vol. 2, no. 9, pp. 4463–4468, 2010.

[21] S. Yoshima, Y. Tanaka, N. Kataoka, N. Wada, J. Nakagawa, and K. Kitayama, "Full-duplex, extended-reach 10G-TDM-OCDM-PON system without En/decoder at ONU," *J. Lightw. Technol.*, vol. 31, no. 1, pp. 43–49, Jan. 2013.

[22] N. Kataoka, G. Cincotti, N. Wada, and K. Kitayama, "2.56 Tbps (40-Gbps $\times$ 8-wavelength $\times$ 4-OC $\times$ 2-POL) asynchronous WDM-OCDMA-PON using a multi-port encoder/decoder," in *Proc. Eur. Conf. Opt. Commun.*, Sep. 2011, pp. 1–3, Paper Th.13.B.6.

[23] E. Wong, "Next-generation broadband access networks and technologies," *J. Lightw. Technol.*, vol. 30, no. 4, pp. 597–608, Feb. 2012.

[24] T. Kodama, Y. Tanaka, S. Yoshima, N. Kataoka, J. Nakagawa, S. Shimizu, N. Wada, and K. Kitayama, "Scaling the system capacity and reach of a 10G-TDM-OCDM-PON system without an en/decoder at an ONU," *J. Opt. Commun. Netw.*, vol. 5, no. 2, pp. 134–143, Feb. 2013.

[25] S. Kobayashi, S. Kutsuzawa, K. Sasaki, H. Iwamura, N. Minato, and A. Nishiki, "Demonstration of 80-km-long SMF transmission on time-spread wavelength-hopping-type OCDM with dispersion compensators," *IEEE. Photon. Technol. Lett.*, vol. 19, no. 18, pp. 1350–1352, Sep. 2007.

[26] J. Kim and C. Park, "Optical design and analysis of CWDM upstream TWDM PON for NG-PON2," *J. Opt. Fiber. Technol.*, vol. 19, no. 3, pp. 250–258, Jun. 2013.

[27] S. Yamashita, T. Yoshida, S. Set, P. Polynkin, and N. Peyghambarian, "Passively mode-locked short-cavity 10GHz Er:Yb-codoped phosphate-fiber laser using carbon nanotubes," in *Proc. SPIE.*, Jan. 2007, vol. 6453, pp. Y1–Y9.

[28] R. Kashyap, *Fiber Bragg Grating*, 1st ed. ed. New York, NY: USA Academic, 1993.

[29] X. Wang, K. Matsushima, A. Nishiki, N. Wada, and K. Kitayama, "High reflectivity superstructured FBG for coherent optical code generation and recognition," *Opt. Exp.*, vol. 12, no. 22, pp. 5457–5468, Nov. 2004.

[30] C. Lam, *Passive Optical Networks*, 1st ed. ed. New York, NY, USA: Academic, 2007.

Ryosuke Matsumoto received the B.E. and M.E. degrees from Osaka University, Osaka, Japan, in 2011 and 2012, respectively. He is currently working toward the Dr. Eng. degree at the same University. He is the Sudent Member of the Institute of Electronics, Information and Communication Engineers (IEICE) in Japan.

Takahiro Kodama (S'11–M'12) received the B.E. degree from Ritsumeikan University, Shiga, Japan, in 2008, and the M.E. and Dr. Eng. degrees from Osaka University, Osaka, Japan, in 2010 and 2012, respectively. In 2012, he was selected as a Research Fellow of the Japan Society for the Promotion of Science. His research interests include optical signal processing, optical access network, and optical packet switching network. Dr. Kodama is a Member of the Institute of Electronics, Information and Communication Engineers (IEICE) of Japan. He received the 2011 IEEE Kansai Section Student Paper Award from the IEEE.

Satoshi Shimizu received the B.E., M.E., and Ph.D. degrees from Tokyo Institute of Technology in 2004, 2006, and 2011, respectively. He was engaged in optical label processing for optical packet switching systems, and all-optical signal processing technology for achieving flip-flop operation. Since 2011, he is with the National Institute of Information and Communications Technology. His research interests include all-optical OFDM and optical signal processing. Dr. Shimizu is a member of IEEE Photonics Society, Japan Society of Applied Physics, Institute of Electronics, Information and Communication Engineers.

Ryujiro Nomura received the B.E. and M.E. degrees from the University of Tokyo, Tokyo, Japan, in 2008 and 2011, respectively. In 2011, he joined Fujikura Ltd., Koto-ku, Tokyo, Japan, where he has been engaged in research and development of fiber Bragg grating.

Koji Omichi received the B.E. and M.E. degrees in material engineering from Shizuoka University, Shizuoka, Japan, in 1999 and 2001, respectively. In 2001, he joined Fujikura Ltd., Koto-ku, Tokyo, Japan, where he has been engaged in research and development of fiber Bragg grating, fiber optic sensor and other optical devices. Mr. Omichi is the Member of the Institute of Electronics, Information and Communication Engineers (IEICE) of Japan and the Japan Society of Applied Physics.

Naoya Wada (M'97) received the B.E., M.E., and Dr. Eng. degrees in electronics from Hokkaido University, Sapporo, Japan, in 1991, 1993, and 1996, respectively. In 1996, he joined the Communications Research Laboratory (CRL), Ministry of Posts and Telecommunications, Tokyo, Japan. He has been the Project Reader of Photonic Node Project and Research Manager of NICT from 2006. Since April 2009, he has been a Group Reader of the Photonic Network Group. His current research interests include the area of photonic networks and optical communication technologies, such as optical switching network, energy-efficient network, optical access system, optical processing system, burst-mode optical communication technologies, and optical packet and optical circuit integrated network. He has published more than 100 papers in refereed English journals and more than 300 papers in refereed international conferences. Dr. Wada received the 1999 Young Engineer Award from the Institute of Electronics, Information and Communication Engineers of Japan (IEICE), and the 2005 Young Researcher Award from the Ministry of Education, Culture, Sports, Science and Technology, Japan. He is a member of IEEE Comsoc, IEEE Photonics, IEICE, the Japan Society of Applied Physics (JSAP), and the Optical Society of Japan (OSJ).

Ken-Ichi Kitayama (S'75–M'76–SM′89–F'03) received the M.E. and Dr. Eng. degrees in communication engineering all from Osaka University, Osaka, Japan, in 1976 and 1981, respectively. In 1976, he joined the NTT Laboratory. From 1982 to 1983, he was a Research Fellow at the University of California, Berkeley, CA, USA. In 1995, he joined the Communications Research Laboratory (presently, NICT). Since 1999, he has been the Professor at the Department of Electrical, Electronic and Information Engineering, Graduate School of Engineering, Osaka University. His research interests include photonic label switching, optical signal processing, next-generation optical access systems, and radio-over-fiber communications. He has published about 280 papers in refereed journals, written a book, two book chapters, and translated one book. He holds more than 30 patents. He currently serves as the Associate Editor of IEEE/OSA JOURNAL OF LIGHTWAVE TECHNOLOGY and *Journal of Optical Communications and Networking* as the Associate Editor. He is the Fellow of the IEICE.